

Many-Body Dissipative Particle Dynamics Simulations of Lipid Bilayers with the MDPD-MARTINI Force-Field

Natalia Kramarz†, Luís H. Carnevale†, and Panagiotis E. Theodorakis

Institute of Physics, Polish Academy of Sciences,

Al. Lotników 32/46, 02-668 Warsaw, Poland

* *Email Address: panos@ifpan.edu.pl*

†: *equal contribution*

(Dated: January 3, 2025)

Many-body dissipative particle dynamics (MDPD) offers a significant speed-up in the simulation of various systems, including soft matter, in comparison with molecular dynamics (MD) simulations based on Lennard-Jones interactions, which is crucial for describing phenomena characterized by large time and length scales. Moreover, it has recently been shown that the MARTINI force-field coarse-graining approach is applicable in MDPD, thus rendering feasible the simulation of complex systems as in MD MARTINI for ever larger systems for longer physical times. Here, simulations of various lipid membranes were performed by using the MDPD-MARTINI coarse-grained (CG) force-field, relevant properties were calculated, and comparison with standard MD MARTINI CG simulations and experimental data was made. Thus insights into structural properties of these bilayer systems and further evidence regarding the transferability of the MDPD-MARTINI models are provided. In this regard, this is a natural next step in the development of the general-purpose MDPD-MARTINI CG force-field, which generally provides significant speed-ups in both computational and physical simulated times, in comparison with standard CG MD simulations.

Keywords: Many-Body Dissipative Particle Dynamics, Molecular Dynamics, MARTINI Force-Field, Lipid Bilayers

I. INTRODUCTION

Molecular dynamics (MD) [1] is a common method used for the simulation of a whole range of materials in various areas, such as soft matter, fluid dynamics, and solid-state physics. A key element for reliable MD simulations is the ability of describing the interactions between particles (force field) in such a way that various experimental properties of interest of a system are well-reproduced by the simulation. To this end, the non-bonded interactions between particles play a key role in reproducing these properties and much of the research for creating the various force-fields (FFs) is mainly focused on adequately describing those non-bonded interactions for a given cutoff at a specific temperature (the development of FFs valid over a wide range of temperatures is an active field of research), with further refinements coming from the topology FF parameters. When interactions are considered between all atoms of the system, that is in the case of all-atom FFs, simulations are generally computationally expensive, albeit often necessary, for example, when a finer time- and length-scale resolution is required, what has led to the development of coarse-grained (CG) FFs [2–5]. In this case, interactions between group of atoms are modeled instead of individual atoms, thus the number of required force (interactions) calculations during the integration of the equations of motion in MD simulations is significantly reduced, which, in turn, results in faster simulations and significant savings in energy resources consumed to run the simulations and cool down the hardware. Moreover, CG models offer the possibility of using a larger time step in the simulation and faster dynamics, which provides an additional speed-up of the simulations.

MARTINI is one of the most popular CG FFs for MD simulation, since it is a general-purpose FF that can be applied in the simulation of a wide spectrum of components [6–9], such as proteins [10–13], polymers [14], carbohydrates [15], glycolipids [16], glycans [17], DNA [18], RNA [19], water [20] and various solvents [21]. In addition, various extensions include simulations for specific pH [22] and more recently chemical reactions (reactive MARTINI) [23]. While the MARTINI 3.0 FF [24] has recently been released, the development of any FF is a continuous effort that aims at improving the FF parameters through refinement based on a wider range of methodologies and validation with experimental data on an ever growing number of possible systems. In the case of CG FFs, validation can often take place by comparison to results obtained by well-established all-atom FFs or CG models.

Regarding the MARTINI MD FF, its popularity is mainly due to the fact that it allows for the simulation of a wide spectrum of different systems by only using a finite number of CG bead types

and a top-down approach for non-bonded interactions. Here, the concept of a 'LEGO' approach of combining these beads to build more complex molecules while accounting for chemical specificity is used. In addition, MARTINI is based on the Lennard-Jones potential with the smallest possible cutoff including attractions, which, in principle, renders this model computationally efficient, while various features implemented in GROMACS software (e.g. virtual atoms) [25], namely the native platform for MARTINI, allow for further speed-up of the simulations. Currently, the MD MARTINI method enjoys a large community, which applies and further tests the models in a range of diverse systems, thus practically participating in the validation effort of this general-purpose FF.

Despite the wide use of the MD MARTINI model, MD is still a computationally expensive method, even for CG models. However, it has recently been shown that the MARTINI approach can be applied in the case of many-body dissipative particle dynamics (MDPD) [26], a method that offers a computational speed-up of about an order of magnitude in comparison with the MD method due to the short-range interactions, as well as an additional speed-up from the use of soft interactions, while at the same time it accounts for both repulsion and attraction between particles [27–32]. Moreover, there is no limitation in combining MDPD and MD models in the same simulation. However, such a scenario is in general undesirable, since it will naturally incur a higher computational cost for the simulation. Here, we build on previous work that dealt with the study of DPPC bilayers and further apply the MDPD-MARTINI FF in investigating POPC and DOPC lipid bilayers and compare the obtained results with those of standard MD-MARTINI simulations. Such a comparison between the MD and MDPD MARTINI FFs is realized on the basis of a number of related properties for bilayer systems. Moreover, a new interaction level is provided to account for the C3 MARTINI bead-type in DOPC and POPC lipids. The MDPD-MARTINI models provides equivalent results to the MD MARTINI models, while they offer at the same time a significant speed-up in the simulations, namely several minutes of MDPD simulations instead of several hours of MD simulations, while interactions are transferable as in the case of MD MARTINI.

In the following, we present the MDPD- and MD-MARTINI models for the various lipid systems and details on the simulation methods. Then, we present the analysis and discussion of various properties. In the last section, we draw our conclusions and discuss next steps in the development of the general-purpose MDPD-MARTINI FF.

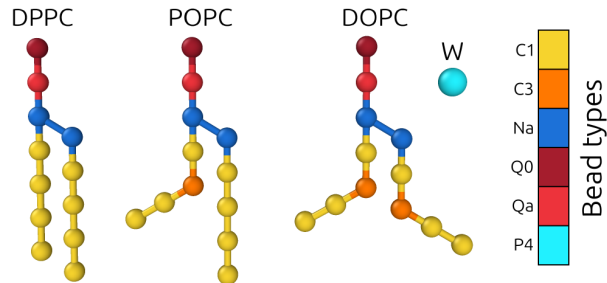


FIG. 1. MD and MDPD models of DPPC, DOPC and POPC lipids. The type of beads are indicated by the different color. In particular, Q_0 represents the choline headgroup, Q_a the phosphate headgroup, two N_a beads correspond to the glycerol ester moiety, while the two alkane chains consist of C_1 and C_3 (for POPC and DOPC) beads. The POPC has a double bond at carbon atom positions 9 and 10, while the DOPC has a double bond at each chain, as illustrated. The interactions between the beads are given in Table II.

II. SIMULATION MODELS AND METHODS

A. Molecular Dynamics

The MD model follows that of previous work for DPPC bilayers [26], which has been a benchmark system in the case of the MD MARTINI FF [33] and therefore further details will be here omitted. Initial files for LAMMPS software [34, 35] for the DPPC, DOPC, and POPC bilayers based on the MD-MARTINI model can be found as moltemplate examples [36]. The DPPC model consists of different bead types, that is Q_0 for the choline headgroup, Q_a for the phosphate headgroup, two N_a beads for the glycerol ester moiety, and two chains, each comprised of four C_1 beads, to represent the alkane tails. For DOPC and POPC lipids, the model differs from that of DPPC lipids. This distinction arises due to the presence of double bonds in the alkane chains, with one double bond in POPC and two in DOPC. These double bonds require a different angle in the chain structure and an additional bead type, C_3 , to accurately represent their molecular geometry. The lipid models are illustrated in **Figure 1**, with the names of the bead types being the same for both the MD and MDPD MARTINI models following the MARTINI FF naming convention. Hence, this implies that both models use the same mapping of CG beads to chemical group of atoms. Finally, water is represented by the P4 bead type.

Typical simulations for forming the lipid bilayers follow the same protocol as in previous work

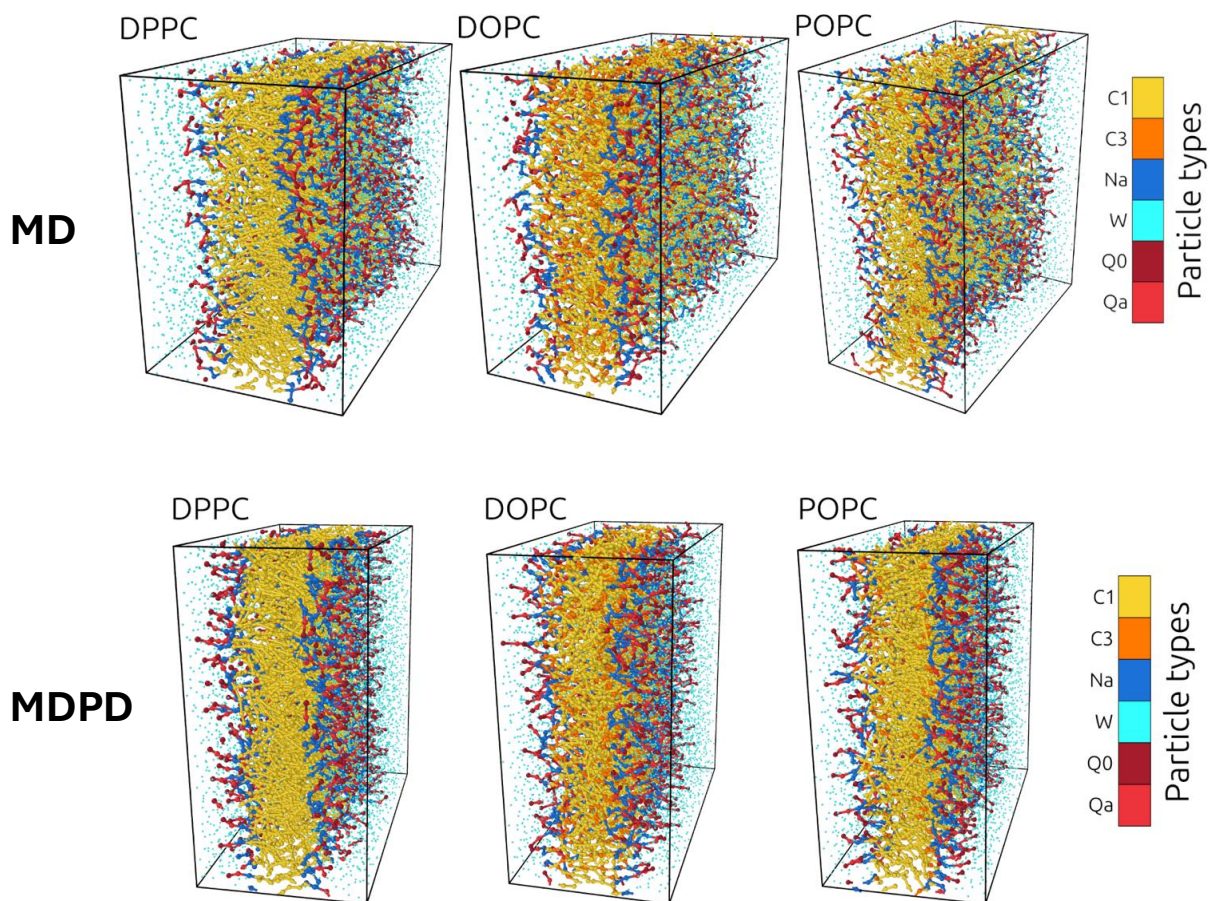


FIG. 2. Typical snapshots of DPPC, DOPC, and POPC bilayers of 512 lipids in water. Upper panel corresponds to results obtained by MD-MARTINI FF simulations, while the lower panel refers to simulated structures obtained via the MDPD-MARTINI force-field.

[26]. However, here, the aim is not to show the computational speed-up of the method during the bilayer formation, since this is well-established for MDPD simulations and becomes even apparent during the calculation of the system properties after the system has reached equilibrium, but rather to assess the quality performance of the MDPD-MARTINI model in the simulation of DOPC and POPC bilayers with an additional C3 bead-type and investigate key properties of these bilayers. Typically, the simulated systems consist of 512 lipids, which are placed in a simulation box of dimensions $L_x = L_y = 130$ and $L_z = 100$, maintaining a 16:1 proportion of water beads.

Preparing the bilayers involves minimizing the system's energy, conducting a simulation in the NPT ensemble employing the Nosé–Hoover thermostat at 300 K and 1 bar to obtain the equilibrium

box volume. Then, simulations are carried out at an elevated temperature (typically around 450 K) to facilitate the removal of any undesired structures that may have formed, and the final bilayer formation. Further refinement of the system can take place by realizing NPT simulations employing a zero surface tension condition while gradually lowering the temperature to 300 K. Equilibrium properties are calculated by NPT runs at this temperature with typical snapshots for each system presented in **Figure 2**.

B. Many-body dissipative particle dynamics

The MDPD method has been applied for fluids with different properties [28–32, 37–39], as well as a range of soft matter multi-phase and multi-component systems, such as systems with surfactant molecules [40, 41]. The most common use of MDPD simulation is usually carried out by solving the Langevin equation of motion for each particle (**Equation 1**) as is also done in the case of MD simulations [42]. However, in the case of MDPD, forces are directly defined, instead of being provided by a potential form. The positions and velocities of each particle evolve according to Equation 1

$$m \frac{d\mathbf{v}_i}{dt} = \sum_{j \neq i} \mathbf{F}_{ij}^C + \mathbf{F}_{ij}^R + \mathbf{F}_{ij}^D, \quad (1)$$

which considers the interactions of a particular particle i with all surrounding particles within a cutoff distance, \mathbf{F}^C , and the presence of dissipative, \mathbf{F}^D , and random forces, \mathbf{F}^R , to act as a thermostat. The mass m is the same for all particles and set to unity.

The total conservative force on particle i , namely, \mathbf{F}^C , which is the main difference between dissipative particle dynamics (DPD) and MDPD [43–47] is mathematically expressed by the following relation

$$\mathbf{F}_{ij}^C = A\omega^C(r_{ij})\mathbf{e}_{ij} + B(\bar{\rho}_i + \bar{\rho}_j)\omega^d(r_{ij})\mathbf{e}_{ij} \quad (2)$$

and includes attractive ($A < 0$) and repulsive ($B > 0$) interactions. r_{ij} is the distance between particles, \mathbf{e}_{ij} the unit vector connecting particles i and j , while $\omega^C(r_{ij})$ and $\omega^d(r_{ij})$ are linear weight functions given as

$$\omega^C(r_{ij}) = \begin{cases} 1 - \frac{r_{ij}}{r_c}, & r_{ij} \leq r_c \\ 0, & r_{ij} > r_c. \end{cases} \quad (3)$$

r_c is a cutoff distance for the interactions, which is usually set to unity. Moreover, $\omega^d(r_{ij})$ has the same form, but its cutoff distance is $r_d = 0.75$. The repulsive term in the conservative force

depends on the local densities, which are expressed as follows:

$$\bar{\rho}_i = \sum_{0 < r_{ij} \leq r_d} \frac{15}{2\pi r_d^3} \left(1 - \frac{r_{ij}}{r_d}\right)^2. \quad (4)$$

The random and dissipative forces are

$$\mathbf{F}_{ij}^D = -\gamma \omega^D(r_{ij}) (\mathbf{e}_{ij} \cdot \mathbf{v}_{ij}) \mathbf{e}_{ij}, \quad (5)$$

$$\mathbf{F}_{ij}^R = \xi \omega^R(r_{ij}) \theta_{ij} \Delta t^{-1/2} \mathbf{e}_{ij}, \quad (6)$$

respectively, with γ being the dissipative strength, ξ the strength of the random force, \mathbf{v}_{ij} the relative velocity between particles, and θ_{ij} a random variable from a Gaussian distribution with unit variance. The fluctuation–dissipation theorem requires that γ and ξ be related by the following relation

$$\gamma = \frac{\xi^2}{2k_B T}. \quad (7)$$

The temperature of the system in the simulations was $T = 1$ (MDPD units) while the weight functions for the dissipative and random forces are

$$\omega^D(r_{ij}) = [\omega^R(r_{ij})]^2 = \begin{cases} \left(1 - \frac{r_{ij}}{r_c}\right)^2, & r_{ij} \leq r_c \\ 0, & r_{ij} > r_c. \end{cases} \quad (8)$$

The equations of motion (**Equation 1**) are integrated by a modified velocity-Verlet algorithm in LAMMPS [34, 35] with a time step $\Delta t = 0.01$. The non-bonded interactions between beads are tuned by varying A_{ij} , while repulsive interactions will remain constant as $B = 35$ [48]. In the MDPD model, harmonic bond and angle interactions are employed, which are mathematically expressed as

$$E_{bond} = k (r_{ij} - r_0)^2, \quad (9)$$

and

$$E_{angle} = k_A (\theta_{ijk} - \theta_0)^2, \quad (10)$$

respectively. The parameters for the bond interactions are $k = 150$ and $r_0 = 0.5$, while for the angles $k_A = 5$, while θ_0 depends on the specific molecule with values indicated in **Table I**.

The MDPD model for the DPPC, POPC, and DOPC is illustrated in **Figure 1**. Moreover, the interactions between the different beads are presented in **Table II** [26]. Also, an additional

Angle	θ_0
$Q_0 - Q_a - N_a$	I
$Q_a - N_a - N_a$	II
$Q_a - N_a - C_1$	I
$N_a - N_a - C_1$	II
$N_a - C_1 - C_3$	I
$N_a - C_1 - C_1$	I
$C_1 - C_3 - C_1$	II
$C_3 - C_1 - C_1$	I
$C_1 - C_1 - C_1$	I

TABLE I. θ_0 values for equilibrium angles for triads of consecutive CG beads: 180° (I); 120° (II).

	P4	Q0	Qa	Na	C_1	C_3
P4	I	I	I	II	VI	V
Q0	I	IV	IV	II	VI	V
Qa	I	IV	IV	II	VI	V
Na	II	II	II	III	VI	V
C_1	VI	VI	VI	VI	VI	VI
C_3	V	V	V	V	VI	VI

TABLE II. Interaction matrix for parametrized MDPD beads organized in six interaction levels (I-VI) with corresponding attractive parameters (A): -50 (I); -43 (II); -34 (III); -30 (IV); -28 (V); -26 (VI).

bead-type C3 with respect to the DPPC lipid model has been considered as in the MD-MARTINI model in the case of the DOPC and POPC lipids. Finally, forming the bilayers by using the MDPD-MARTINI model follows the same simulation protocol as in the MD-MARTINI simulations with temperature increase from 300 K to 450 K. Typical snapshots for each bilayer case obtained from MDPD simulations are presented in **Figure 2** alongside the corresponding MD-MARTINI snapshots.

III. RESULTS AND DISCUSSION

The MD and MDPD MARTINI systems typically consisted of 512 lipids, while in certain cases, for example, for determining the spectrum intensities of the undulation modes on the bilayer, larger systems have been used (8192 lipids in total). Firstly, the area per lipid (APL) was examined. This can be determined by the area a lipid covers in such bilayers, in other words, this is the area of the

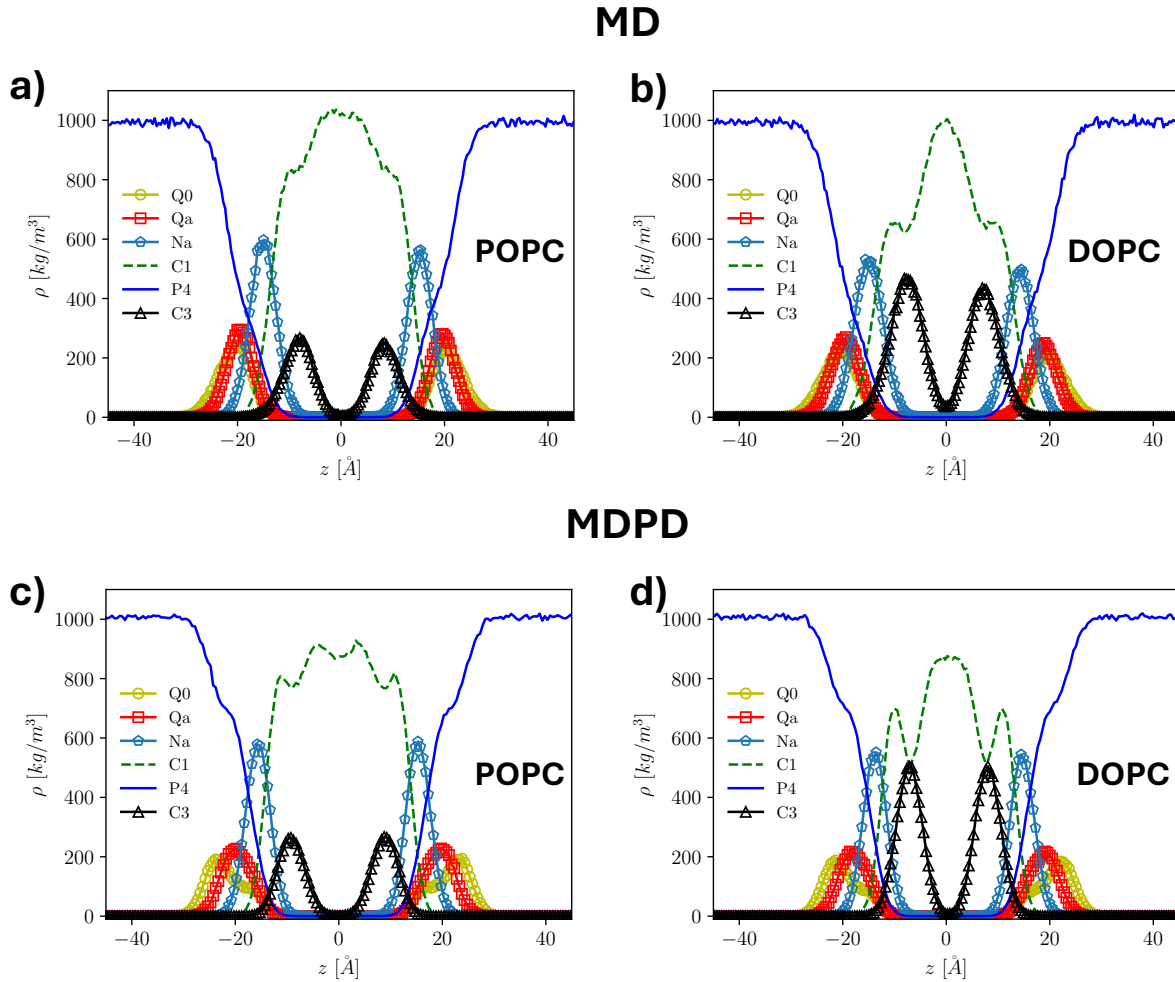


FIG. 3. Comparison of bilayer thickness in MD (a, b) and MDPD (c, d) models. Results for POPC (a, c) and DOPC (b, d) bilayers consisting of 512 lipid molecules are shown. The values of bilayer thickness are reported in Table IV.

bilayer divided by the average number of lipids in a single monolayer. In our study, the area of a plane aligned tangentially to the bilayer surface in the simulation box was divided by half the total number of lipid molecules in order to calculate the APL. This property depends on various factors, such as the lipid type and temperature. In this case, the influence of the lipid type was examined and a comparison between the MD and MDPD models was performed. The exact values of APL for DPPC, POPC, and DOPC bilayers are reported in Table III. In particular, we can observe that APL values are in good agreement in both models, with the APL decreasing in the case of POPC and DOPC lipid bilayers. This is expected partly due to the different angle involving the C3-type beads (Table I).

Lipid	MD	MDPD
DPPC	60.8	55.6
POPC	51.1	49.1
DOPC	49.8	52.6

TABLE III. Area per lipid (APL) for each bilayer system obtained through MD and MDPD simulations in \AA^2 .

Lipid	MD	MDPD
DPPC	42.5	42.8
POPC	40.3	41.7
DOPC	39.1	41.7

TABLE IV. Values of bilayer thickness for each lipid in \AA .

Another fundamental property that has been estimated is the thickness bilayer for the different lipids for both the MDPD- and MD-MARTINI models. This parameter is essential for describing structural aspects of the bilayers and was determined by identifying the peaks in the density distribution profile of the choline head-group bead (Q_0) as shown in Figure 3. It is found that both the MD and MDPD models are in agreement with each other and moreover with experimental data [49] for all lipid bilayer cases. The exact values are reported in Table IV. In particular, it has been found that the thickness exhibits minor differences in the different systems. Only a slight decrease in the thickness is observed in the case of POPC and DOPC bilayers, while the structural characteristics expressed through the density profiles of each bilayer for the various bead types are similar for both the MD and the MDPD models, as shown in Figure 3.

Lipid bilayers possess elastic properties, which can be expressed by the bending modulus, k_c . In particular, this reflects the intensity of undulations within the lipid membrane and can be obtained by the fluctuation spectrum [50]. By replicating the bilayers in the bilayer plane and running short simulations to reach equilibrium structures, the undulation spectrum was determined. Specifically, undulations can be described through a surface function, $u(x, y)$, which represents the average position of the two monolayers based on the positions of the phosphate head beads. Then, the undulation spectrum, \hat{u} , can be obtained by performing a Fourier transform on the surface function, that is:

$$\hat{u}(\mathbf{q}) = \frac{1}{N} \int u(\mathbf{x}) e^{-i\mathbf{q}\cdot\mathbf{x}} d\mathbf{x}. \quad (11)$$

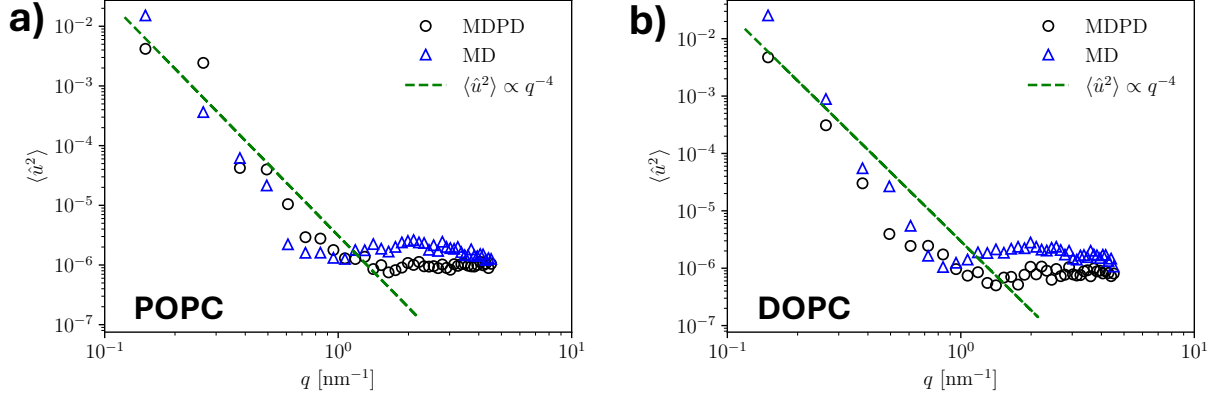


FIG. 4. Spectrum intensities of the undulation modes on the bilayer. Long wavelengths obey the q^{-4} behavior and transition around an 1 nm wavelength to a constant value in both the MD and the MDPD simulations is observed for POPC (a) and DOPC (bilayers). Data are obtained for a system of 8192 lipids.

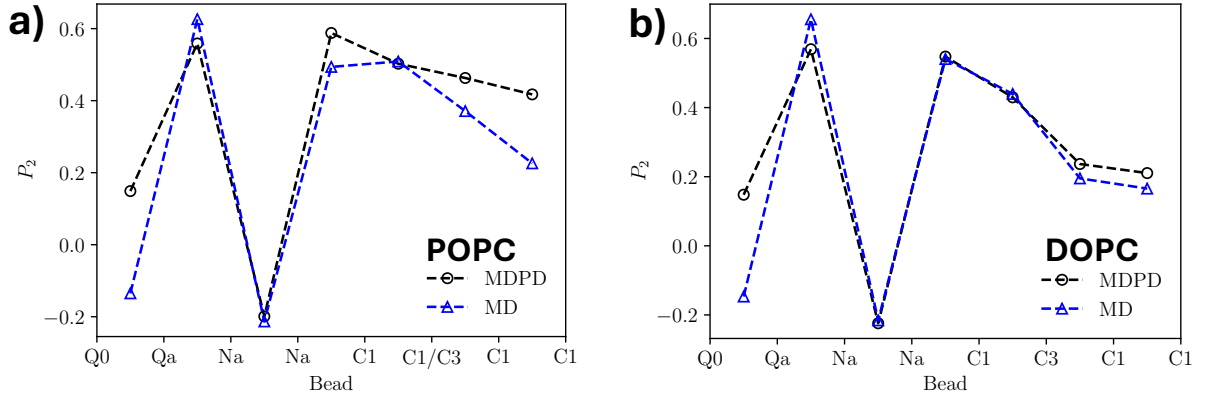


FIG. 5. Second-rank order-parameter, P_2 , calculated for every bond along the lipid molecule in the case of POPC and DOPC lipids. Each bilayer consisted of 8192 lipids.

Moreover, the undulation intensities in the Fourier space are expected to follow the relation [50]

$$\langle \hat{u}^2 \rangle = \frac{k_B T}{A} \left(\frac{1}{k_c q^4} + \frac{1}{\gamma q^2} \right), \quad (12)$$

where $A = L_x L_y$ is the lipid-membrane area, while $q = |\mathbf{q}| = \sqrt{q_x^2 + q_y^2}$ is the wavevector length in the radial direction and γ the surface tension. Our data, shown in Figure 4, for the DOPC and POPC bilayers exhibit the q^{-4} scaling for the long wavelength modes, with a very good match between the MD and the MDPD results. Moreover, in comparison with previous results for DPPC bilayers [26], here, the q^{-2} dependence is not present due to the application of the zero surface-tension condition. The q^{-4} dashed line was plotted by considering the experimentally obtained bending modulus $k_c = 5^{-20} \text{J}$ [51].

To further compare the MD- and MDPD-MARTINI results, the second-rank order parameter P_2 was computed, given by the following relation:

$$P_2 = \frac{1}{2} (3\langle \cos^2 \theta \rangle - 1) \quad (13)$$

Here, θ is the angle between each bond and the bilayer normal direction. Thus, it describes the alignment of the lipid molecules. In particular, values closer to $P_2 = 1$ indicate a higher degree of alignment with the normal direction, whereas values around $P_2 = 0$ rather point to a random orientation. Finally, values towards $P_2 = -0.5$ indicate anti-alignment. The obtained results indicate that the MDPD-MARTINI model can reproduce the alignment characteristics of the lipid molecules as in the MD simulations.

IV. CONCLUSION

The MDPD-MARTINI FF was employed for investigating structural properties of lipid bilayers with results being compared to simulations based on the widely used MD-MARTINI CG FF. The two models are in very good agreement in a range of different properties discussed in this study, thus providing further support in favor of using MDPD models, since simulations are much faster in terms of computational time and even more in terms of the simulated physical time of the systems. This particular feature opens the door for reaching larger systems and longer times scales in the simulation of complex systems, covering the full-range of chemical groups currently available in the MD-MARTINI models. This will also have the potential of accelerating the acquisition of physical-based data, which can be used in machine learning or other artificial-intelligence methods. Moreover, the FF parameters of the C3 MARTINI bead-type has been provided to the MDPD-MARTINI interaction matrix [26]. In view of the transferability of the potential based on the hydrophobic/hydrophilic characteristics of chemical groups represented by the CG beads, which is an important concept in the MARTINI coarse-graining approach and demonstrated here in the case of DPPC, POPC, and DOPC lipids. Thus, a range of different systems can be simulated by the provided set of interactions by following the MARTINI mapping of CG beads to chemical units for a range of different systems and additional ones can be investigated for further validations.

Acknowledgments

This research has been supported by the National Science Centre, Poland, under grant No. 2019/34/E/ST3/00232. We gratefully acknowledge Polish high-performance computing infrastructure PLGrid (HPC Center: ACK Cyfronet AGH) for providing computer facilities and support

within computational grant no. PLG/2023/016608.

Conflict of interest

There is no conflict of interest.

- [1] D. C. Rapaport, *The Art of Molecular Dynamics Simulation*, 2nd ed. (Cambridge University Press, 2004).
- [2] W. G. Noid, Perspective: Coarse-grained models for biomolecular systems, *J. Chem. Phys.* **139**, 090901 (2013).
- [3] S. Kmiecik, D. Gront, M. Kolinski, L. Wieteska, A. E. Dawid, and A. Kolinski, Coarse-grained protein models and their applications, *Chem. Rev.* **116**, 7898 (2016).
- [4] J. Jin, A. J. Pak, A. E. P. Durumeric, T. D. Loose, and G. A. Voth, Bottom-up coarse-graining: Principles and perspectives, *J. Chem. Theory Comput.* **18**, 5759 (2022).
- [5] W. G. Noid, Perspective: Advances, challenges, and insight for predictive coarse-grained models, *J. Phys. Chem. B* **127**, 4174 (2023).
- [6] S. J. Marrink, A. H. de Vries, and A. E. Mark, Coarse grained model for semiquantitative lipid simulations, *J. Phys. Chem. B* **108**, 750 (2004).
- [7] S. J. Marrink, H. J. Risselada, S. Yefimov, D. P. Tieleman, and A. H. de Vries, The martini force field: Coarse grained model for biomolecular simulations, *J. Phys. Chem. B* **111**, 7812 (2007).
- [8] S. J. Marrink and D. P. Tieleman, Perspective on the martini model, *Chem. Soc. Rev.* **42**, 6801 (2013).
- [9] R. Alessandri, F. Grünewald, and S. J. Marrink, The martini model in materials science, *Adv. Mat.* **33**, 2008635 (2021).
- [10] L. Monticelli, S. K. Kandasamy, X. Periole, R. G. Larson, D. P. Tieleman, and S.-J. Marrink, The martini coarse-grained force field: Extension to proteins, *J. Chem. Theory Comput.* **4**, 819 (2008).
- [11] X. Periole, M. Cavalli, S.-J. Marrink, and M. A. Ceruso, Combining an elastic network with a coarse-grained molecular force field: Structure, dynamics, and intermolecular recognition, *J. Chem. Theory Comput.* **5**, 2531 (2009).
- [12] D. H. de Jong, G. Singh, W. F. D. Bennett, C. Arnarez, T. A. Wassenaar, L. V. Schäfer, X. Periole, D. P. Tieleman, and S. J. Marrink, Improved parameters for the martini coarse-grained protein force field, *J. Chem. Theory Comput.* **9**, 687 (2013).
- [13] A. B. Poma, M. Cieplak, and P. E. Theodorakis, Combining the martini and structure-based coarse-grained approaches for the molecular dynamics studies of conformational transitions in proteins, *J. Chem. Theory Comput.* **13**, 1366 (2017).
- [14] H. Lee, A. H. de Vries, S.-J. Marrink, and R. W. Pastor, A coarse-grained model for polyethylene oxide and polyethylene glycol: Conformation and hydrodynamics, *J. Phys. Chem. B* **113**, 13186 (2009).
- [15] C. A. López, A. J. Rzepiela, A. H. de Vries, L. Dijkhuizen, P. H. Hünenberger, and S. J. Marrink,

- Martini coarse-grained force field: Extension to carbohydrates, *J. Chem. Theory Comput.* **5**, 3195 (2009).
- [16] C. A. López, Z. Sovova, F. J. van Eerden, A. H. de Vries, and S. J. Marrink, Martini force field parameters for glycolipids, *J. Chem. Theory Comput.* **9**, 1694 (2013).
- [17] S. Chakraborty, K. Wagh, S. Gnanakaran, and C. A. López, Development of Martini 2.2 parameters for N-glycans: a case study of the HIV-1 Env glycoprotein dynamics, *Glycobiology* **31**, 787 (2021).
- [18] J. J. Uusitalo, H. I. Ingólfsson, P. Akhshi, D. P. Tieleman, and S. J. Marrink, Martini coarse-grained force field: Extension to dna, *J. Chem. Theory Comput.* **11**, 3932 (2015).
- [19] J. J. Uusitalo, H. I. Ingólfsson, S. J. Marrink, and I. Faustino, Martini coarse-grained force field: Extension to rna, *Biophys. J.* **113**, 246 (2017).
- [20] S. O. Yesylevskyy, L. V. Schäfer, D. Sengupta, and S. J. Marrink, Polarizable water model for the coarse-grained martini force field, *PLOS Comput. Biol.* **6**, 1 (2010).
- [21] P. Vainikka, S. Thallmair, P. C. T. Souza, and S. J. Marrink, Martini 3 coarse-grained model for type iii deep eutectic solvents: Thermodynamic, structural, and extraction properties, *ACS Sustain. Chem. Eng.* **9**, 17338 (2021).
- [22] F. Grünewald, P. C. T. Souza, H. Abdizadeh, J. Barnoud, A. H. de Vries, and S. J. Marrink, Titratable Martini model for constant pH simulations, *J. Chem. Phys.* **153**, 024118 (2020).
- [23] S. Sami and S. J. Marrink, Reactive martini: Chemical reactions in coarse-grained molecular dynamics simulations, *J. Chem. Theory Comput.* **19**, 4040 (2023).
- [24] P. C. T. Souza, R. Alessandri, J. Barnoud, S. Thallmair, I. Faustino, F. Grünewald, I. Patmanidis, H. Abdizadeh, B. M. H. Bruininks, T. A. Wassenaar, P. C. Kroon, J. Melcr, V. Nieto, V. Corradi, H. M. Khan, J. Domański, M. Javanainen, H. Martinez-Seara, N. Reuter, R. B. Best, I. Vattulainen, L. Monticelli, X. Periole, D. P. Tieleman, A. H. de Vries, and S. J. Marrink, Martini 3: a general purpose force field for coarse-grained molecular dynamics, *Nat. Methods* **18**, 382 (2021).
- [25] H. Berendsen, D. van der Spoel, and R. van Drunen, Gromacs: A message-passing parallel molecular dynamics implementation, *Comput. Phys. Commun.* **91**, 43 (1995).
- [26] L. H. Carnevale and P. E. Theodorakis, Many-body dissipative particle dynamics with the martini lego approach, *Eur. Phys. J. Plus* **139**, 539 (2024).
- [27] I. Pagonabarraga and D. Frenkel, Dissipative particle dynamics for interacting systems, *J. Chem. Phys.* **115**, 5015 (2001).
- [28] P. B. Warren, Vapor-liquid coexistence in many-body dissipative particle dynamics, *Phys. Rev. E* **68**, 066702 (2003).
- [29] J. Zhao, S. Chen, and N. Phan-Thien, Viscometric flow for a many-body dissipative particle dynamics (mdpd) fluid with lees-edwards boundary condition, *Mol. Sim.* **44**, 213 (2017).
- [30] J. Zhao, S. Chen, K. Zhang, and Y. Liu, A review of many-body dissipative particle dynamics (mdpd): Theoretical models and its applications, *Phys. Fluids* **33**, 112002 (2021).
- [31] C. Zhao, J. Zhao, T. Si, and S. Chen, Influence of thermal fluctuations on nanoscale free-surface flows:

- A many-body dissipative particle dynamics study, *Phys. Fluids* **33**, 112004 (2021).
- [32] Y. Han, J. Jin, and G. A. Voth, Constructing many-body dissipative particle dynamics models of fluids from bottom-up coarse-graining, *J. Chem. Phys.* **154**, 084122 (2021).
- [33] Martini tutorials: lipids with the lipidome (), www.cgmartini.nl/index.php/tutorial/37-tutorial2/356-tutorial-lipids-new-lipids, accessed 25.09.2023.
- [34] S. Plimpton, Fast parallel algorithms for short-range molecular dynamics, *J. Comp. Phys.* **117**, 1 (1995).
- [35] A. P. Thompson, H. M. Aktulga, R. Berger, D. S. Bolintineanu, W. M. Brown, P. S. Crozier, P. J. in 't Veld, A. Kohlmeyer, S. G. Moore, T. D. Nguyen, R. Shan, M. J. Stevens, J. Tranchida, C. Trott, and S. J. Plimpton, LAMMPS - a flexible simulation tool for particle-based materials modeling at the atomic, meso, and continuum scales, *Comput. Phys. Commun.* **271**, 108171 (2022).
- [36] Moltemplate examples (), https://www.moltemplate.org/visual_examples.html, accessed 27.09.2023.
- [37] P. Español and P. Warren, Statistical mechanics of dissipative particle dynamics, *Europhys. Lett. (EPL)* **30**, 191 (1995).
- [38] P. Vanya, P. Crout, J. Sharman, and J. A. Elliott, Liquid-phase parametrization and solidification in many-body dissipative particle dynamics, *Phys. Rev. E* **98**, 033310 (2018).
- [39] L. H. Carnevale, P. Deuar, Z. Che, and P. E. Theodorakis, Liquid thread breakup and the formation of satellite droplets, *Phys. Fluids* **35**, 074108 (2023).
- [40] R. L. Hendrikse, C. Amador, and M. R. Wilson, A many-body dissipative particle dynamics parametrization scheme to study behaviour at air–water interfaces, *Soft Matter* **19**, 3590 (2023).
- [41] L. H. Carnevale, P. Deuar, Z. Che, and P. E. Theodorakis, Surfactant-laden liquid thread breakup driven by thermal fluctuations, *Phys. Fluids* **36**, 033301 (2024).
- [42] P. E. Theodorakis, W. Paul, and K. Binder, Analysis of the cluster formation in two-component cylindrical bottle-brush polymers under poor solvent conditions. a simulation study, *Eur. Phys. J. E* **34**, 52 (2011).
- [43] P. Español and P. B. Warren, Perspective: Dissipative particle dynamics, *J. Chem. Phys.* **146**, 150901 (2017).
- [44] Y. Yoshimoto, I. Kinefuchi, T. Mima, A. Fukushima, T. Tokumasu, and S. Takagi, Bottom-up construction of interaction models of non-markovian dissipative particle dynamics, *Phys. Rev. E* **88**, 043305 (2013).
- [45] Z. Li, X. Bian, B. Caswell, and G. E. Karniadakis, Construction of dissipative particle dynamics models for complex fluids via the mori–zwanzig formulation, *Soft Matter* **10**, 8659 (2014).
- [46] E. Lavagnini, J. L. Cook, P. B. Warren, and C. A. Hunter, Translation of chemical structure into dissipative particle dynamics parameters for simulation of surfactant self-assembly, *J. Phys. Chem. B* **125**, 3942 (2021).
- [47] S. Y. Trofimov, E. L. F. Nies, and M. A. J. Michels, Constant-pressure simulations with dissipative particle dynamics, *J. Chem. Phys.* **123**, 144102 (2005).

- [48] P. B. Warren, No-go theorem in many-body dissipative particle dynamics, *Phys. Rev. E* **87**, 045303 (2013).
- [49] D. Drabik, G. Chodaczek, S. Kraszewski, and M. Langner, Mechanical properties determination of dmpe, dppc, dspc, and hspc solid-ordered bilayers, *Langmuir* **36**, 3826 (2020).
- [50] P. Tarazona, E. Chacón, and F. Bresme, Thermal fluctuations and bending rigidity of bilayer membranes, *J. Chem. Phys.* **139**, 094902 (2013).
- [51] W. Rawicz, K. Olbrich, T. McIntosh, D. Needham, and E. Evans, Effect of chain length and unsaturation on elasticity of lipid bilayers, *Biophys. J.* **79**, 328 (2000).